

Suspended sediment concentration estimation in the Sacramento-San Joaquin Delta of California using long short-term memory networks

Han Sang Kim  | Minxue He  | Prabhjot Sandhu

California Department of Water Resources,
Sacramento, California, USA

Correspondence

Minxue He, California Department of Water Resources, 1516 9th Street, Sacramento, CA 95618, USA.

Email: kevin.he@water.ca.gov

Abstract

Sedimentation is an important aspect of water resources management with many implications. Often, process-based methods are employed to predict and assess the amount of sediment in water, but there are still challenges because the mechanisms that govern sediment transport are not yet fully understood. Furthermore, complex domains make model calibration difficult. Thus, as a complementary tool, a machine-learning model was developed in the present study to emulate an existing process-based model in simulating suspended sediment concentration (SSC). It employs the long short-term memory (LSTM) networks, which are a type of artificial neural networks (ANNs) designed for supervised learning of a sequence of data (e.g., time series). The model was applied to the Sacramento-San Joaquin Delta (the Delta) of California, USA, which is characterized by an interconnected system of sloughs, waterways, and a tidal outlet. The model training was performed with historical records of flow, stage and SSC at various locations within the Delta. The study period was 2010 through 2016, but the training period (i.e., range of observed data used to train the model) was varied to assess the model's sensitivity to the inputs and to determine the optimum model setup. Comparison between the model-estimated SSC and the observation at 12 key locations within the Delta showed that the estimation accuracy of the LSTM model during the study period is comparable or superior to that of the Delta Simulation Model II-General Transport Model (DSM2-GTM), a process-based operational hydrodynamics and water quality model for the Delta. In terms of the ratio of the root-mean-square error to the standard deviation (RSR), LSTM models generally showed higher predictability than DSM2-GTM in all test cases investigated, with the lowest (most desirable) and highest (least desirable) LSTM-based RSR being 0.21 and 1.14, respectively. In comparison, the lowest and highest RSR values with DSM2-GTM were 0.26 and 3.70, respectively. The median LSTM-based RSR of all study locations is around 0.7 while its DSM2-GTM counterpart is about 1.0. LSTM models also yielded remarkably higher (more desirable) Nash-Sutcliffe Efficiency values. Moreover, visual inspection found that LSTM models better captured the timing and magnitude of peaks as well as the temporal variations in the SSC time series. The LSTM model's performance was further analysed with hydro-meteorological data (precipitation and wind speed) incorporated in

training. While precipitation led to some improvement, the wind speed was found to have a negligible effect overall. All in all, the study findings suggest that the LSTM model has the potential to supplement the operational process-based model in guiding water resources planning and management practices.

KEY WORDS

long short-term memory networks, machine learning, Sacramento-san Joaquin Delta, sediment

1 | INTRODUCTION

1.1 | Background

1.1.1 | Sediment and society

It is a well-known fact that the first civilizations were established around rivers, for the abundance of water enabled our ancestors to raise crops and livestock. However, an equally important environmental factor was the sediment, which often formed literally the building blocks of those civilizations and without which agriculture would have been unattainable (Dartnell, 2019). Many millennia have passed since, but sediment still plays a critical role in shaping societies. For instance, deltaic communities are in constant threat from erosion, and their areas are affected by changes in sediment flux due to human activities such as dam constructions (Nienhuis et al., 2020). Severe soil loss around bridge piers can lead to failures, which can result in loss of lives (Hunt, 2009). High concentration of suspended sediment in drinking water may pose health risks (WHO, 2017). Thus, it is essential to develop methods and technologies to assess, predict, and manage sediment and related processes.

There are many natural factors that can initiate and influence sediment processes in aquatic environments. Rainfall is a major one, which induces surface erosion (Kim et al., 2021; Thomas et al., 2018; Vendramini et al., 2018). Wind can cause turbulence in waters, which disturbs the sediment on bed to increase suspended sediment concentration (Wang et al., 2020). With aeolian transport, wind can also directly introduce sediment into bodies of water (Eichmanns & Schüttrumpf, 2020). In estuarine and marine environments, the combined effects of waves and currents govern sediment processes (Seymore, 1989). Anthropogenic activities also contribute to sediment processes, in the form of construction (Aoula et al., 2021), dredging (Pastor et al., 2020), propeller wash (Yew et al., 2017), and beach nourishment (Choi et al., 2018), to name a few.

1.1.2 | Sacramento-San Joaquin Delta

Sediment plays a critical role in deltaic areas, including the Sacramento-San Joaquin Delta (the Delta), the largest delta on the western coast of the United States (Figure 1). Situated between the Sierra Nevada and the San Francisco Bay, the Delta plays an important role as a water and ecological resource; roughly 25 million Californians rely on the Delta as their water source (Klausmeyer & Fitzgerald, 2012), and it is a habitat to diverse wildlife (SFEI-

ASC, 2016). One notable characteristic of the Delta is that it consists of an interconnected system of rivers, canals, reservoirs, and a tidal outlet. Moreover, it has been heavily altered by anthropogenic activities, notably hydraulic mining, construction of dams and levees, groundwater pumping, and dredging, which have huge implications on sediment transport in the region (Bernard et al., 2013).

What makes the Delta a particularly interesting site is its hydrology; several major rivers flow into the Delta from the east and there is constant tidal forcing from the Pacific Ocean to the west, while water also leaves the system as exports to other regions within California. Within the Delta boundaries, there is a network of waterways that transports water and suspended sediment. Such complexity often poses a burden to traditional process-based models, which require extensive calibration.

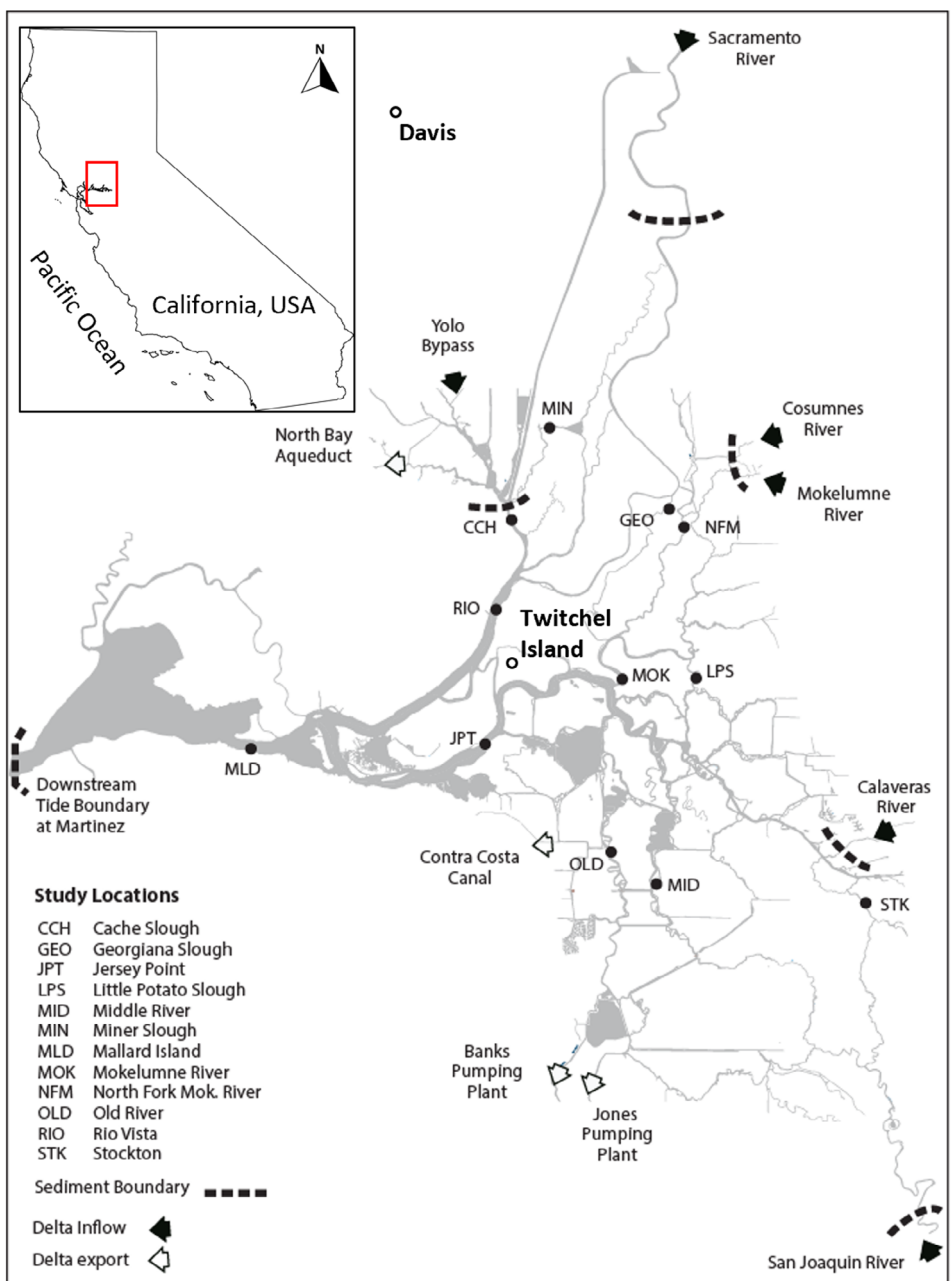
1.2 | Literature review

1.2.1 | Sediment in the Delta

The Delta is an estuary, which is marked by complex sediment processes driven by interaction between rivers and the sea (Prentice et al., 1968; Seymore, 1989). Given the important role the Delta plays as described in the preceding section, proper sediment management is key for the well-being of the communities and ecosystem within and surrounding it (Schoellhamer et al., 2012). One implication of local sediment processes is a light limitation caused by high-suspended sediment concentration (SSC) impacting primary productivity in the water column (Jassby et al., 2002). Sediment resuspension can also cause the contaminants previously deposited in the sediment bed to be released back into the water column (Kalnejais et al., 2007).

There have been holistic approaches to understanding the sediment processes in the Delta system. Schoellhamer et al. (2012) adopted a conceptual model to summarize sedimentation in the region and found that a majority of sediment transport occurs during wet periods as suspended load. Bernard et al. (2013) conducted a comprehensive provenance study by integrating various techniques that consider biological composition, in-situ flow measurements and numerical modelling. On the other hand, McKee et al. (2013) analysed station records at various locations in the Central Valley watershed to identify source of sediment and suggested that small tributaries may account for the majority of sediment flux into the Delta. Marineau and Wright (2014) found that human alteration of the Delta's landscape affected its hydrodynamics and sediment transport.

FIGURE 1 Map of the Delta showing major locations and features that are of interest to the study. The inset map shows the relative location of the Delta in the State of California, United States



Despite its importance to the Delta, the corresponding SSC field data at multiple locations in the Delta only became available recently. The SSC data are collected and managed by the United States Geological Survey (USGS). The time series of SSC are obtained through regression equations using in-stream turbidity measurements (Buchanan & Morgan, 2014). Two different types of instruments can be deployed to measure turbidity: optical backscatter sensor or nephelometric sensor (Rasmussen et al., 2009). Sensors are typically positioned at two depths (one near water surface and the other near the bottom) at most stations to capture the vertical variability. The specific depths depend on the tidal stage range at each station and vary across different stations. In order to calibrate the regression equations, in-situ water samples are collected routinely (but much less frequently than the automatic turbidity sensors') with horizontally

positioned Van Dorn-style sampler (Buchanan & Morgan, 2014) to analyse the concentration of suspended sediment. In turn, the concentration of sediment is determined through a procedure designed to extract only the particles classified as sediment and remove salts (Fishman & Friedman, 1989).

1.2.2 | Numerical modelling of sediment transport in the Delta

In order to predict sediment processes in fine temporal and spatial scales, researchers have also utilized process-based models for numerical simulation, aided by recent development of powerful yet inexpensive computing tools (MacWilliams et al., 2016). Bever et al. (2013)

used a coupled hydrodynamic (UnTRIM), wind wave (SWAN), and sediment transport (SediMorph) to simulate sediment transport in the San Pablo Bay, and found that local sediment flux cannot be described with depth-averaged current speed alone. Erikson et al. (2013) utilized the Delft3D model to develop an equation that relates suspended sediment flux at the Golden Gate in terms of the sediment concentration at Alcatraz Island and the tide-averaged currents computed from tidal constituents. The model was first calibrated and validated with sediment concentration measurements. Delft3D was also used by Achete et al. (2015) to simulate suspended sediment transport in the Bay-Delta system. Using this approach, the amount of time it takes for sediment to travel from the Sacramento River to key locations was determined.

However, because the mechanisms governing sediment transport are not yet fully understood and due to the Delta system's complexity, more research is needed to improve the performance of process-based methods for the entire Delta region.

1.2.3 | Artificial neural networks

In addition to process-based models, data-driven approaches such as artificial neural networks (ANNs) have also been applied in sediment simulation (Afan et al., 2016). The plain form of an ANN is called a multi-layer perceptron (MLP). An MLP utilizes a network structure to implicitly derive the relationships between one or more inputs (e.g., flow observations) and outputs (e.g., SSC at locations of interest). The network structure typically consists of an input layer, an output layer, and one (or more) hidden layer(s). The basic processing units in each layer are called neurons. Neurons in the input layer feed input information to neurons in the following hidden layer, which then outputs a transformation of the combined inputs to neurons in the next layer. The connections between neurons in two adjacent layers are represented by linear weights. These weights are mutable network parameters determined via a process called *training*. The training process aims to minimize the difference (i.e., error signal) between network estimations (e.g., on SSC) and the corresponding field measurements. The most widely used training approach is probably the gradient descent approach. This approach propagates the error signal backward into the network and updates the weights based on the chain rule until preset training thresholds or criteria are met (Rumelhart et al., 1986).

One drawback of MLP is that it does not consider the sequential ordering of input data. For variables that have temporal dependencies with input data (e.g., the current SSC depends on current flow rate as well as antecedent flow conditions), MLPs may not be ideal. A special type of ANN, recurrent neural networks (RNNs), can explicitly treat temporal ordering by recurrently feeding the output of a neuron in the hidden layer as an additional input to itself in the next time-step. That being understood, conventional RNNs have difficulties in preserving long-term dependencies, as the error signal can be back propagated effectively only for a few steps (Bengio et al., 1994). Different variants of RNNs have been developed to better capture long-term

dependencies between input and output variables. The most popular variant is probably the deep learning long-short term memory (LSTM) network (Hochreiter & Schmidhuber, 1997).

Different from the standard RNN, LSTM implements the concept of gates into the network structure. These gates are basically neurons with learnable weights. A typical LSTM contains three types of gates (forget, input, and output) that inform the network on what information to remove, what to add, and what to output. This gate configuration enables the network to preserve essential information contained in the input times series for a long time. LSTM networks have only been recently applied in the Delta simulating the flow and salinity relationships (He et al., 2020).

It should be pointed out that there are other statistical methods capable of capturing time-dependent patterns in time series. One common approach is the Fourier spectral analysis, which can be used to determine the frequency of a phenomenon occurring in the time domain (Brigham, 1988). Although versatile in its application, Fourier spectral analysis can only be used on statistically stationary data (Davoodi et al., 2009). Hence, as an alternative, researchers have utilized wavelet transformation, which is capable of processing non-stationary time series (Juez et al., 2021). In fact, temporal information obtained from the Fourier spectral analysis or wavelet transformation can be used to inform machine-learning models. This will be further discussed later in the paper.

1.3 | Study scope

This study can be considered as a proof-of-concept, whereby machine learning models are developed as a complementary tool to emulate an existing process-based model to simulate the transport of suspended sediment in the Delta. More specifically, the models employ long short-term memory (LSTM) Networks, a special type of artificial neural network (ANN). The machine learning models (hereafter referred to as "LSTM models") estimate suspended sediment concentration (SSC) at a number of key stations within the Delta. The process-based Delta Simulation Model II-General Transport Model (DSM2-GTM) is selected as the performance benchmark for the LSTM models to emulate. Several training–testing schemes (ratios of available data used for training and testing of model) were applied to the LSTM models to explore the model performance. Additionally, the impact of hydro-meteorological processes including precipitation and wind speed on the performance of LSTM models are assessed. This present effort is unique in that state-of-the-art machine learning methods were employed to estimate SSC in the Delta for the first time. In short, this study pursues the following research objectives:

1. Develop a data-driven model for suspended sediment concentration estimation, which would emulate and complement conventional process-based methods.
2. Improve model performance by adopting different training–testing schemes.

3. Assess the impact of incorporating hydro-meteorological processes (precipitation and wind speed) on the model performance.

2 | METHODOLOGY

2.1 | DSM2-GTM

2.1.1 | Overview

The benchmark model with which the LSTM models will be compared is DSM2-GTM. DSM2-GTM is a numerical model developed by the California Department of Water Resources to simulate transport of waterborne materials (e.g., sediment) in the Delta channels (Hsu et al., 2016; Hsu et al., 2019). Employing the one-dimensional form of the advection-dispersion-reaction equation in a Eulerian mesh, it considers the material being transported as a scalar quantity. In the case of suspended sediment, this means that it represents the amount of sediment in water as a concentration instead of tracking the movement of particles. The flow field required to compute the advection and diffusion is provided by the hydrodynamics module of DSM2. For detailed descriptions on the governing sediment transport equation of DSM2-GTM, the readers are referred to Hsu et al. (2019).

As a process-based model developed primarily for Delta applications, the domain for DSM2-GTM consists of nodes that represent various locations within the Delta. These locations are connected by segments, which represent channels and waterways. With the assumption of one-dimensional flow, DSM2-GTM can efficiently determine the flow and the sediment concentration by solving the equations that govern the transport. Recently, DSM2-GTM was extensively calibrated for erosion coefficient with both sand and fine particles (Abrishtamchi & Nam, 2019). For past applications of DSM2-GTM, please refer to CDWR (2016) and CWC (2016).

2.1.2 | Sediment characteristics

DSM2-GTM requires specification of the sediment characteristics that reflect the study environment. Thus, we used USGS sediment data to specify the ratios of sand and fines at the inlet boundaries (Hsu et al., 2019). In the current research, the suspended sediment was represented with two particle sizes: 0.0625 and 0.004 mm for sand and fines, respectively. The simplification of using only two sediment sizes was necessary to reduce the computing time to run the model; processing the dynamics among the entire array of field-observed particle sizes would make the computing time prohibitively long. Secondly, as much as we want to fully capture the Delta's sediment characteristics; there is simply no complete record of sediment distribution across the domain, especially interior Delta (Hsu et al., 2019).

2.2 | LSTM models

In this study, LSTM models were developed through supervised learning for the purpose of estimating SSC. The learning labels consisted of the SSC at 12 key locations presented in Figure 1 and Table 1. These locations were selected based on data availability and their geographic importance in water resource management. It is worth noting from Table 1 the wide range of learning label values; there is a difference of greater than five orders of magnitude between the maximum SSC observed at MOK and the minimum SSC observed at STK. On the other hand, the feature vectors were various hydraulic and sediment concentration measurements, as tabulated in Table 2. The general trend of the learning labels and training data are shown in Figure 2, which presents the time series of SSC at select stations (MIN, JPT, and MID) and flow rate from the two major inflow locations (Sacramento River at Freeport as the primary flow source and San Joaquin River at Vernalis as the secondary flow source). It can be seen that their large-scale (seasonal and inter annual) temporal trends

TABLE 1 Study stations at which the LSTM models are applied, with maximum, minimum, and mean of field-observed values

Name	Station ID	Max (mg/L)	Min (mg/L)	Mean (mg/L)
Cache Slough at Ryer Island	CCH	148.09	3.18	19.83
Georgiana Slough near Sacramento River	GEO	417.41	3.76	24.34
San Joaquin River at Jersey Point	JPT	51.4	6.9	17.55
Little Potato Slough at Terminus	LPS	52.77	1.63	9.03
Middle River at Middle River	MID	15.24	1.97	6.26
Miner Slough at Highway 84 Bridge	MIN	612.29	0.83	20.77
Sacramento River at Mallard Island	MLD	96.63	14.02	30.37
Mokelumne River at Andrus Island near Terminus	MOK	2169.58	1.15	20.06
North Mokelumne W Walnut Grove Road	NFM	195.62	1.28	11.28
Old River at Bacon Island	OLD	85.19	1.83	9.23
Sacramento River at Rio Vista	RIO	247.73	5.03	23.23
San Joaquin River below Garwood Bridge at Stockton	STK	538.62	0.07	29.75

Abbreviation: LSTM, long short-term memory.

TABLE 2 Inputs for the LSTM model training

Variable (unit)	Description	Location name
Flow (cfs)	Amount of water flowing into the system	Yolo Bypass
		Calaveras River at Stockton
		Cosumnes River
		Mokelumne River at Woodbridge
		Sacramento River at Freeport
		San Joaquin River at Vernalis
Stage (ft)	Height of the surface of water flowing into/out of the system, measured from a datum	Martinez
Diversion (cfs)	Amount of water taken out of the system and used in the watershed	Contra Costa Pumping Plant at Rock slough
		Contra Costa Pumping Plant at Victoria Canal
Export (cfs)	Amount of water taken out of the system and used in other regions	Jones Pumping Plant at Delta-Mendota Canal (DMC)
		Banks Pumping Plant at Clifton Court Forebay
		Old River near Byron
		Barker Slough at North Bay Aqueduct
Suspended Sediment Concentration (mg/L)	Amount of suspended sediment in the water	Sacramento River (at Freeport)
		Vernalis
		Yolo Bypass
		Mokelumne + Calaveras + Cosumnes
		Martinez

Abbreviations: CFS, cubic feet per second; ft, feet; LSTM, long short-term memory; mg/L, milligrams per litre.

are very similar, such as timing of the peaks in a given water year (WY), a period spanning from 1 October to 30 September and designated by the ending calendar year. For instance, in WY 2011, the SSC time series for MIN shows two largest local maxima occurring separately around 1/1/2011 and 4/1/2011, and so do both flow time series. Similarly, in WY 2016, the largest or second largest local maxima for all five-time series are found between 1/1/2016 and 4/1/2016.

All measurements except for the SSC data used in this study were obtained from the California Data Exchange Center (<https://cdec.water.ca.gov/>), and any sub-daily time series were aggregated into daily (which is the study time step) for consistency. In addition to the measurements, a component of this study also utilized the modelled suspended sediment concentration generated by DSM2-GTM, thereby shedding light on the performance of a machine-learning model reinforced with physics-driven simulated data.

This study focused on water years 2011 to 2016 (10/1/2010 through 9/30/2016) and utilized the observation records within to train and test the LSTM models (one LSTM model for each study location). Several combinations of training and testing periods were implemented, as summarized in Table 3. Here, the term “LSTM-Standard” means that the model was trained using the flow and SSC observations listed in Table 2, while “LSTM-GTM” indicates that DSM2-GTM output was incorporated in addition to those.

The training algorithm for the LSTM model was implemented using the TensorFlow machine-learning package (Abadi et al., 2015).

The steps to train and test for each of the stations (see Table 1) are summarized below, with Scenario 1 as an example:

1. Determine the time range of training and testing period, which correspond to the first and latter 50 percent of the station data, respectively. For instance, if the station has SSC observation spanning from 1 October 2010 to 30 September 2016, the training period will be from 1 October 2010 to 30 September 2013, and the testing period will be from 1 October 2013 to 30 September 2016. In turn, the station's SSC observations corresponding to the training period and testing period are represented by y_{train} and y_{test} , respectively. Sub-daily field observation time series are aggregated into daily frequency.
2. Obtain x_{train} and x_{test} , which are the model inputs (see Table 2) corresponding to the respective time periods. For LSTM-GTM, the DSM2-GTM output for each station is included as an additional input. Sub-daily model inputs are aggregated into daily frequency.
3. The LSTM model is trained using the x_{train} and y_{train} , whose lengths are identical.
4. After being trained, the LSTM model generates estimations based on x_{test} . These estimations are then compared with y_{test} .

It should be noted that one separate LSTM model was developed for each study location. The LSTM model contained two LSTM layers and one output layer. For a given study location, four different units (8, 16, 32, and 64) in each LSTM layer were explored under two batch sizes (64 and 128) during the training, yielding a set of 32 LSTM networks. The best-performing network was chosen as the final model for that location. The learning rate was set to 0.01. Early stopping (at epoch 50) was applied to reduce the potential of overfitting. A previous study (He et al., 2020) that employed similar LSTM architecture,

FIGURE 2 Time series of (a) suspended sediment concentration (SSC) at select locations in the study area and (b) flow at primary inflow boundary locations

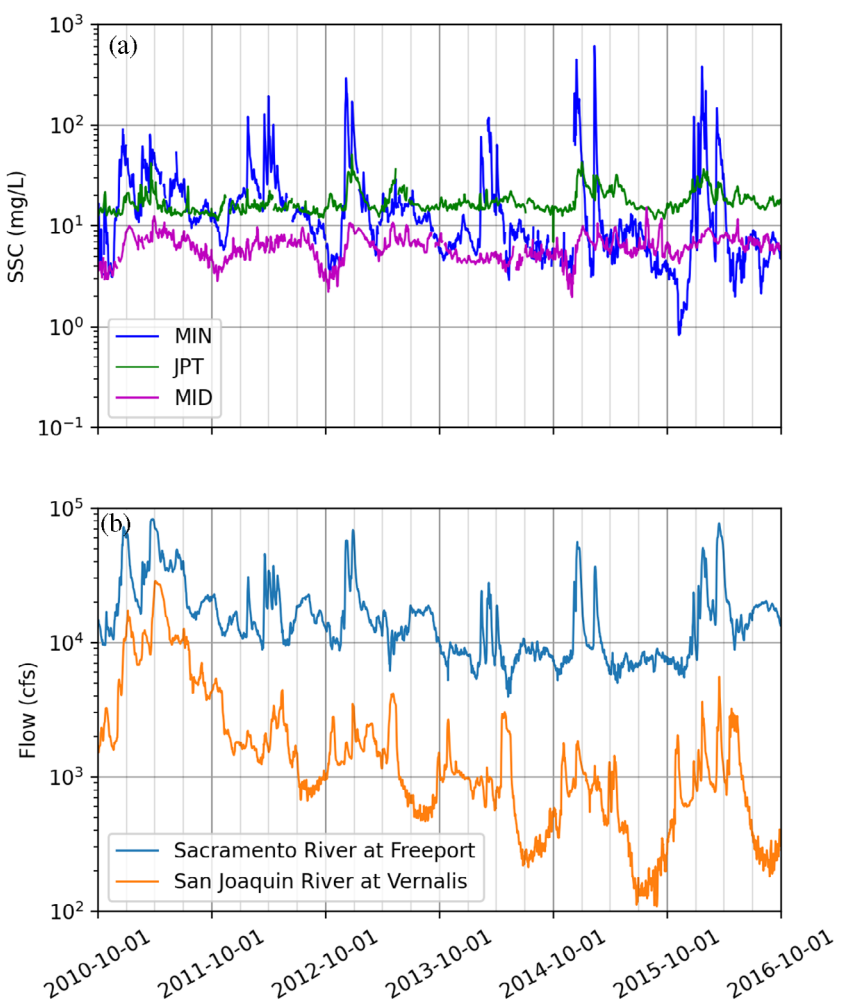


TABLE 3 Training–testing schemes used to develop LSTM models for the estimation of SSC

Scenario ID	Training mode	Training period	Testing period
1	LSTM-standard	First 50% of available station data	Latter 50% of available station data
2	LSTM-standard	First 70% of available station data	Latter 30% of available station data
3	LSTM-standard	Water years 2011–2015	Water year 2016
4	LSTM-GTM	First 50% of available station data	Latter 50% of available station data
5	LSTM-GTM	First 70% of available station data	Latter 30% of available station data
6	LSTM-GTM	Water years 2011–2015	Water year 2016

Note: LSTM-Standard = the model was trained using the flow and SSC observations only; “LSTM-GTM” = DSM2-GTM output was incorporated in addition.

Abbreviations: LSTM, long short-term memory; SSC, suspended sediment concentration.

hyper parameters, and training strategy showed desirable performance for salinity simulation in the same study area.

2.3 | Evaluation metrics

In evaluating the model performance, Nash-Sutcliffe efficiency (NSE) and ratio of root-mean-square error to the standard deviation of the observations (RSR), defined below, were used.

$$NSE = \frac{\sum(O_i - \bar{O})^2 - \sum(P_i - O_i)^2}{\sum(O_i - \bar{O})^2} \quad (1)$$

$$RSR = \frac{RMSE}{STDEV} = \frac{\sqrt{\sum(O_i - P_i)^2}}{\sqrt{\sum(O_i - \bar{O})^2}} \quad (2)$$

where P_i = i -th model-predicted/estimated value, \bar{P} = mean of model-predicted/estimated values, O_i = i -th observed value, \bar{O} = mean of

observed values, RMSE = root mean square error, and STDEV = standard deviation.

Nash-Sutcliffe efficiency (NSE) measures the degree to which the simulated values agree with the observed. Ranging in value between negative infinity and 1, positive NSE indicates that the simulation can fairly mimic the observed data, with NSE = 1 meaning that the simulation and observation are identical. On the other hand, negative NSE indicates that the mean of the observed is a better estimator than the simulation (Golmohammadi et al., 2014). RSR also measures the performance of the simulation. With RMSE as the numerator, a value of zero indicates that RMSE = 0, and that the simulated values are identical to the observed. Conversely, the larger the RSR, the larger the differences are between the simulated and the observed (Golmohammadi et al., 2014) performance.

Furthermore, three additional metrics—standard deviation (STDEV), correlation coefficient (corr), and root-mean-square difference (RMSD)—were determined and displayed in Taylor diagrams (Taylor, 2001). These are defined as:

$$\text{STDEV} = \sqrt{\frac{\sum (P_i - \bar{P})^2}{N}} \quad (3)$$

$$\text{corr} = \frac{\sum (P_i - \bar{P})(O_i - \bar{O})}{\sqrt{\sum (P_i - \bar{P})^2 \sum (O_i - \bar{O})^2}} \quad (4)$$

$$\text{RMSD} = \sqrt{\frac{\sum (P_i - O_i)^2}{N}} \quad (5)$$

where N = number of data points.

Standard deviation (STDEV) measures the amount of variation, or spread, within the predicted/estimated values. The correlation coefficient describes the linear relationship between the predicted/estimated and observed values, with 1 meaning absolute linearity. RMSD, on the other hand, is a measure of the difference between predicted/estimated and observed values, with zero indicating that the two sets are identical.

3 | RESULTS

3.1 | DSM2-GTM model performance

Before gauging the LSTM model's capability in simulating suspended sediment concentration (SSC), the performance of the manually calibrated version of DSM2-GTM in estimating SSC was analysed to create a baseline benchmark. First, as shown in Figures 3 and 4, the statistical metrics NSE and RSR were computed for each of the stations for the three testing periods.

The figures show that the estimation accuracy of DSM2-GTM varies widely across the domain. For instance, while it performed superbly for Georgiana Slough (GEO) (NSE over 0.9 and RSR below 0.3), it essentially had no estimation capability for Middle River (MID)

(negative NSE). In fact, Figure 3 suggests that there is polarization of DSM2-GTM's performance; only in a handful of stations the model estimations can be considered satisfactory or better (Moriasi et al., 2015), and the model adds no value in the rest.

One likely source for such vastly different estimation accuracy is the inherent nature of manual calibration. During calibration of DSM2-GTM (and other manually calibrated mechanistic models), tuning parameters are adjusted, and the impacts on model performance are analysed. This seemingly straightforward procedure can easily turn into an iterative search, where different parts of the domain demand different parameter values. Eventually, a compromise must be made that results in the model under-performing in certain parts. Simply put, it is difficult for mechanistic models to attain the level of model calibration that will ensure satisfactory performance for the entire domain.

3.2 | LSTM model performance

The performance of the LSTM model, in terms of the change in NSE over the DSM2-GTM-based benchmark, is summarized in Figure 5. The LSTM model led to an increase in NSE for all cases except for two (Miner Slough in Scenario 4 and Mokelumne River in Scenario 5). For those stations that improved, the amount of change in NSE varied by orders of magnitude, because NSE has no lower bound and DSM2-GTM resulted in negative NSE. The final NSE values are presented in Figure 6. Comparing with DSM2-GTM-based result (Figure 3), the number of stations with negative NSE has reduced significantly, and the overall improvement is clearly seen.

A similar trend can be found with RSR. Figure 7 presents the percent differences in RSR values over the DSM2-GTM-based benchmark. Here, negative values indicate improved model performance

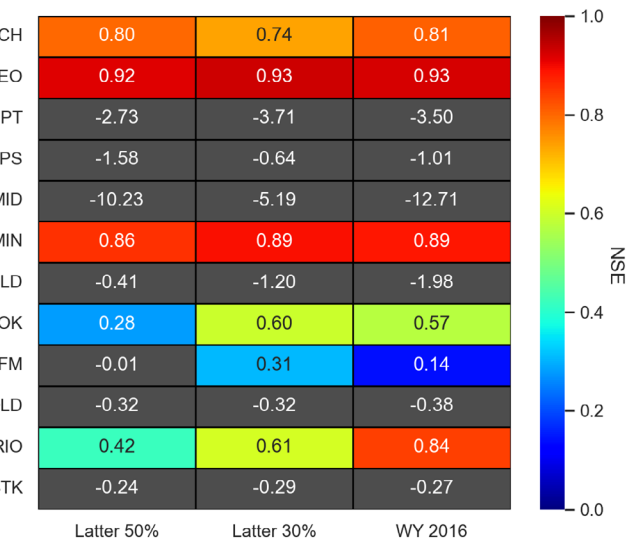


FIGURE 3 Nash-Sutcliffe efficiency (NSE) based on DSM2-GTM. The closer NSE is to 1, the better the model performance. Negative values, which indicate no estimation capability, are coloured in grey



FIGURE 4 Ratios of the root-mean-square error to the standard deviation of the observations (RSR) based on DSM2-GTM. The closer the RSR is to zero, the better the model performance

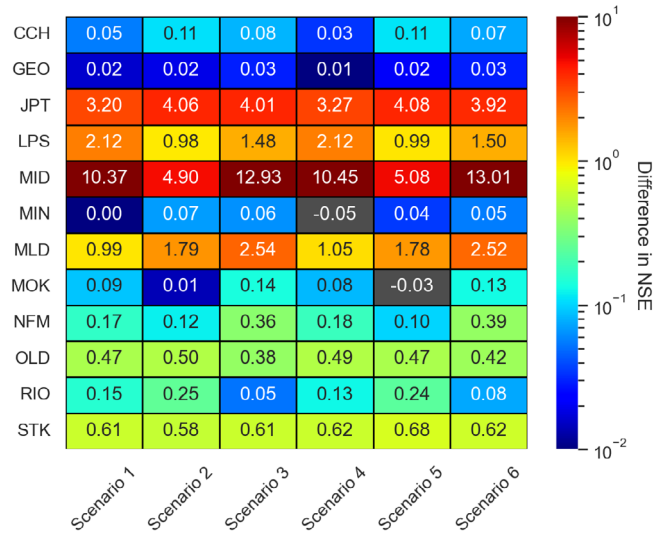


FIGURE 5 Differences between Nash-Sutcliffe efficiency (NSE) values of the long short-term memory (LSTM) model-simulated suspended sediment concentration under different scenarios and their DSM2-GTM counterparts. Positive values indicate improved performance

(RSR = 0 means observation and estimation are identical), and LSTM model performed better except for two cases: Miner Slough (MIN) in Scenario 4 and Mokelumne River (MOK) in Scenario 5. The final RSR values are presented in Figure 8, wherein in general, RSR values are now closer to zero when compared with Figure 4.

While the improved performance over DSM2-GTM is promising, it is interesting to note that further including DSM2-GTM output to the model inputs (i.e., Scenarios 4, 5, and 6) did not guarantee better model performance compared with the scenarios that did not (i.e., Scenarios 1, 2, and 3).

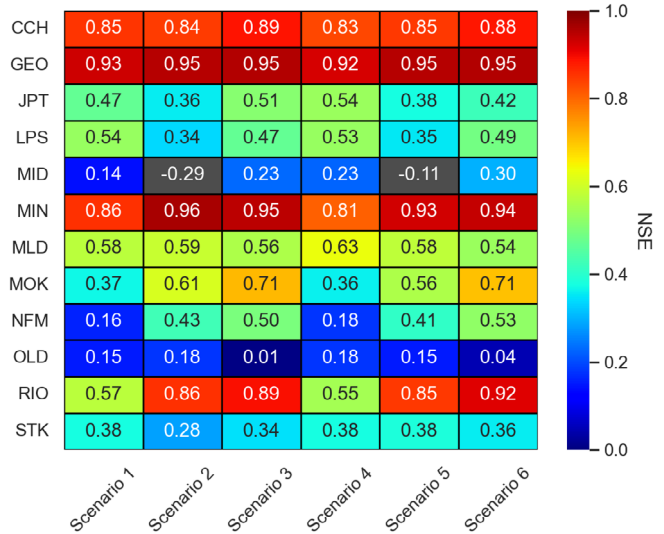


FIGURE 6 Nash-Sutcliffe efficiency (NSE) values of long short-term memory (LSTM) models. The closer NSE is to 1, the better the model performance. Negative values, which indicate no estimation capability, are coloured in grey

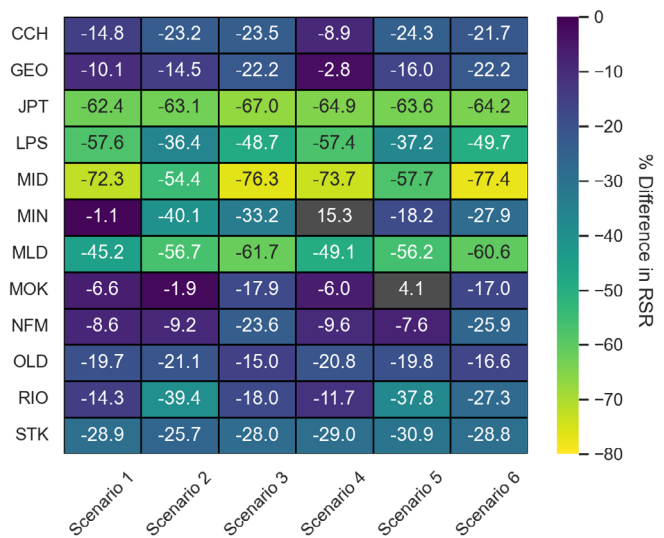


FIGURE 7 Percent differences (%) between ratio of the root-mean-square error to the standard deviation (RSR) values of the long short-term memory (LSTM) model-simulated suspended sediment concentration under different scenarios and their DSM2-GTM counterparts. The greater the magnitude, the better the improvement

In theory, incorporating the output from the process-based model should help reinforce the physical aspect of the process being simulated locally. But LSTM-GTM produced mixed results, even for Miner Slough (MIN), where DSM2-GTM showed good performance. In fact, Figure 5 shows that Scenario 4 actually resulted in decline in model performance. This suggests that human intervention to improve LSTMs may bring adverse effects, and more work is needed on configuring LSTM models.

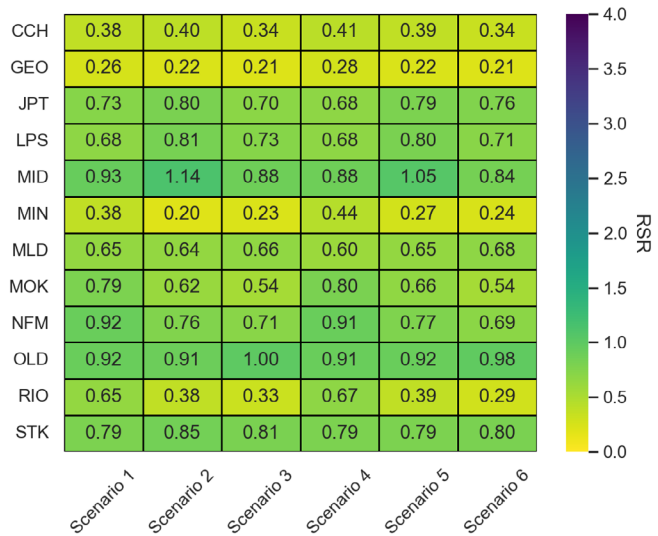


FIGURE 8 Ratios of the root-mean-square error to the standard deviation of the observations (RSR) of long short-term memory (LSTM) models. The closer the RSR is to zero, the better the model performance

To summarize the performance of the different scenarios and determine the best-performing LSTM model setup, the number of stations with best and worst metrics (NSE and RSR) for each scenario are presented in Figure 9. From this figure, it can be deduced that the length of the training data alone is not a sufficient indicator of the model's performance, based on the fact that Scenario 2 (the first 70 percent of available data used for training) produces more stations with worst NSE or worst RSR than Scenario 1 (the first 50 percent of available data used for training) does. But, given that Scenarios 3 and 6 (with a training period of WY 2011 through 2015, which equates to the first 83 percent of available data used for training) both led to more stations with best metrics than those with worst, a longer training period seems to help with model capability in this particular setup.

Figure 9 further investigates the effect of including the DSM2-GTM output as training data. It shows that when 50 percent of the data are used for training, the LSTM-GTM run S4 resulted in significantly more stations with worst metrics (4 bests vs. 10 worsts), while the number of stations with best and worst metrics are almost identical for the Standard run S1 (3 bests vs. 2 worsts). On the other hand, when using 70 percent of the data for training, only one station from S5 is represented in the figure as having the best RSR, making it difficult to compare against the Standard run S2 (4 bests vs. 7 worsts). Lastly, with water years 2011–2015 used for training, the run S6 (8 bests vs. 3 worsts) exhibits more stations with best metrics than the Standard run S3 (4 bests vs. 2 worsts). But in terms of the relative number (i.e., ratio of the number of stations with best metrics to that with worst metrics), the improvement can be interpreted as insignificant. These mixed results suggest that follow-up studies with more stations and other training data are needed to reach a definite conclusion.

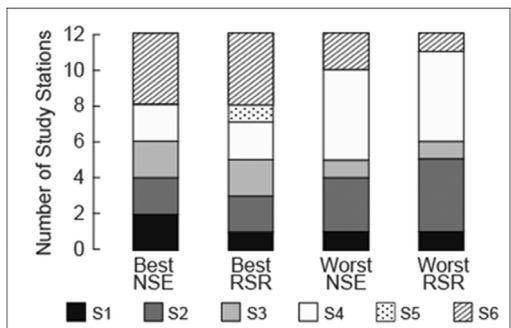


FIGURE 9 Number of stations with the best or worst statistical metrics under each modelling scenario

Figure 10 compares the LSTM model-estimated time series of SSC associated with the highest NSE (among the six scenarios) against the observation and DSM2-GTM output. For simplicity, only a nine-month period spanning from 12/1/2015 to 8/31/2016 is shown for Miner Slough (MIN), San Joaquin River at Jersey Point (JPT), and Middle River (MID), respectively representing higher, intermediate, and lower performance of the LSTM model in matching the observations.

As can be seen in Figure 10, in general, LSTM performed better than DSM2-GTM at estimating suspended sediment concentrations (SSC) in the Delta. It shows that, while both models agree equally well with the observations in their ability to capture the baseline values and the timing of the peaks, LSTM did a better job in capturing the amplitudes of the peaks, particularly from Figure 10b,c.

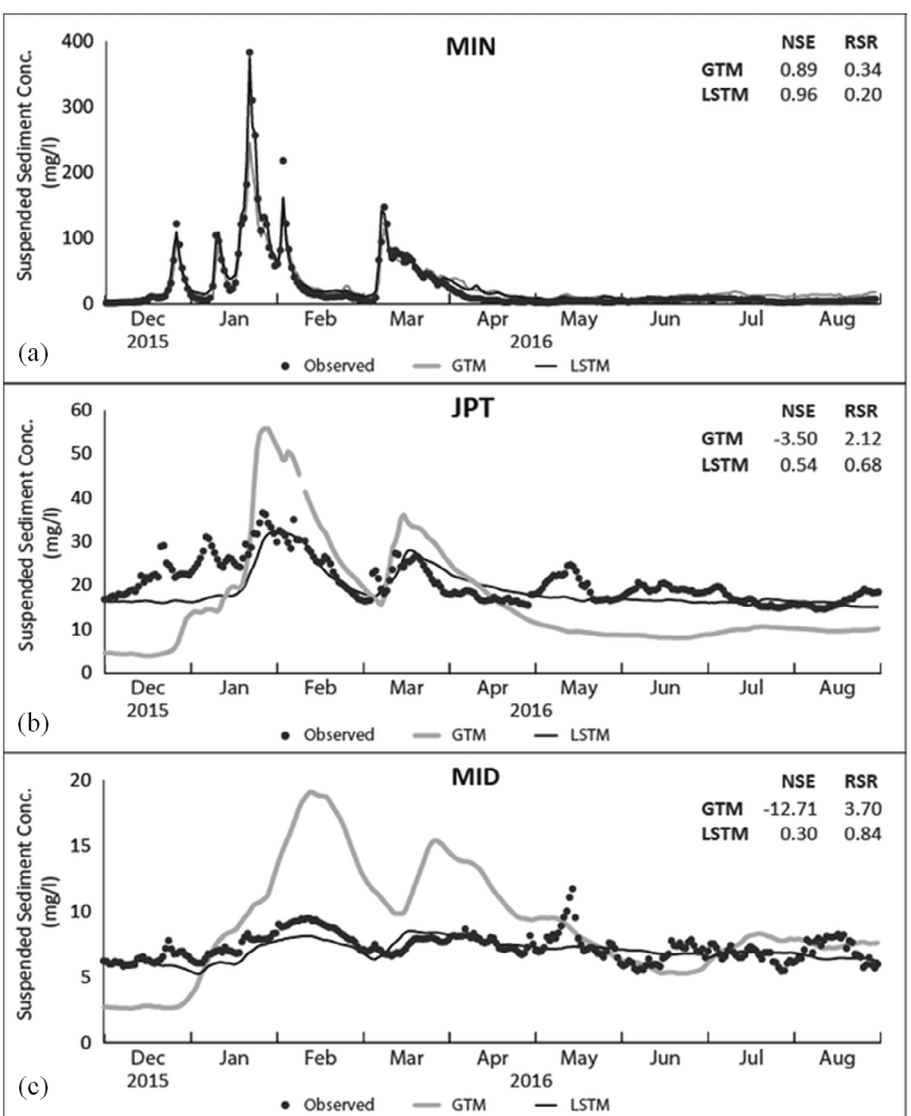
While the tables and figures presented in this section convey that LSTM models have better estimation capability than DSM2-GTM, they are only intended to demonstrate the feasibility of LSTM models. They do not guarantee LSTM models' absolute superiority over DSM2-GTM, and DSM2-GTM may actually show better performance if a different study period or site was selected. DSM2-GTM is also capable of simulating suspended sediment concentrations at numerous locations (versus 12 locations for LSTMs) across the Delta at a much finer scale (e.g., 15-min vs. daily for LSTMs).

4 | DISCUSSIONS

As illustrated in Section 3, including the local suspended sediment concentration generated by DSM2-GTM resulted in mixed findings where the estimation capability did not always improve. As an alternative, other physical variables known to affect sediment transport—precipitation and wind speed—were considered as training inputs. These two variables were chosen among many that contribute to Delta sediment processes (see Section 1.1.1) because there are field measurements available, which can be reliably incorporated into model training and testing. The section first evaluates the impacts of precipitation and wind speed on the performance of LSTM models, respectively. Next, the section discusses limitations of the current work. Lastly, the scientific and practical implications of the study are discussed.

FIGURE 10 Comparison of observed and modelled time series for selected stations with different levels of performance in matching the observation: (a) Miner Slough (MIN), higher performance; (b) San Joaquin River at Jersey Point (JPT), intermediate performance; and (c) Middle River (MID), lower performance. The corresponding metrics are presented in each panel. Disconnected lines indicate that the observations were missing for the corresponding dates, thus no model estimation was made.

GTM = DSM2-GTM



4.1 | Precipitation

Within the study domain, precipitation records are available at seven locations: Brentwood, Davis, Gait, Lodi, Rio Vista, Stockton and Tracy. Because precipitation and SSC time series locations do not coincide, only the precipitation record with highest correlation with the SSC time series was used as the additional input for each study site. It was found that the highest correlations were found with Davis, whose location is shown in Figure 1.

With the additional input of precipitation records, the LSTM models were trained following Scenario 1 for demonstration purposes. Here, the main interest is on whether including precipitation data can improve LSTM model performance, and thus other scenarios were not repeated.

Table 4 presents the correlation with precipitation records, and compares the two NSE values for each study site—one from the “default” run (LSTM-Standard) and the other when precipitation data was included. Similar to the findings for Scenarios 1 through 6, the

changes in NSE varied by stations. However, a general trend was found with stations where the original Scenario 1 exhibited NSE below 0.5 and the correlation between SSC and precipitation is above 0.1: Most of these stations show increase in NSE when precipitation was included, as indicated by the last column. Here, NSE = 0.5 was used as the threshold because it is considered as the minimum for satisfactory fit (Moriasi et al., 2007). For correlation coefficient, 0.1 is the generally accepted limit above which there is a weak but positive relationship (Schobar et al., 2018). While the improvements may not be drastic, this analysis presented precipitation as a potential input that can improve the LSTM models.

4.2 | Wind speed

Next, we considered adding wind data as the additional input for LSTM model training. Unlike precipitation, wind data was found to be low in availability; most of the wind speed time series collected within

TABLE 4 Changes in NSE with precipitation as additional input

Study site	Correlation between SSC and precipitation	NSE-Without precipitation	NSE-With precipitation	Improvement from low NSE (below 0.5)?
CCH	0.139	0.86	0.82	—
GEO	0.204	0.96	0.93	—
JPT	0.169	0.48	0.59	Yes
LPS	0.147	0.4	0.49	Yes
MID	0.007	0.23	0.24	—
MIN	0.162	0.89	0.85	—
MLD	-0.001	0.58	0.54	—
MOK	0.03	0.04	0.03	—
NFM	0.135	0.19	0.2	Yes
OLD	-0.009	0.2	0.2	—
RIO	0.12	0.6	0.58	—
STK	0.148	0.43	0.41	No

Note: The last column indicates whether NSE is improved for stations with an original NSE less than 0.5 and a correlation coefficient greater than 0.1.

Abbreviation: NSE, Nash-Sutcliffe efficiency.

TABLE 5 Changes in NSE with wind speed as additional input

Study site	Correlation coefficient between SSC and wind speed	NSE-Without wind speed	NSE-With wind speed	Improvement from low NSE (below 0.5)?
CCH	-0.01	0.86	0.87	—
GEO	-0.14	0.96	0.95	—
JPT	0	0.48	0.56	—
LPS	-0.08	0.4	0.51	—
MID	0.14	0.23	0.21	No
MIN	-0.1	0.89	0.86	—
MLD	0.17	0.58	0.53	—
MOK	-0.07	0.04	0.03	—
NFM	-0.03	0.19	0.2	—
OLD	0.11	0.2	0.17	No
RIO	-0.08	0.6	0.59	—
STK	0.02	0.43	0.38	—

Abbreviation: NSE, Nash-Sutcliffe efficiency.

the study domain do not go far enough back. In fact, only one station had long enough record. The location of this station (Twitchell Island) is shown in Figure 1.

Similar to precipitation data, Scenario 1 was repeated with the wind speed data as additional inputs. The resulting change in NSE values are tabulated in Table 5, along with the correlation coefficient between SSC and the wind record. Here, we can see that there is negligible or even negative correlation between SSC and wind speed, and that including wind speed did not improve. One explanation is that wind speed varies largely across the Delta, and its impacts are mostly local. Thus, it is not likely that including the one wind speed data at Twitchell Island would benefit SSC estimations far away from it. In fact, there seems to be no significant relationship between the correlation and model change in performance.

4.3 | Taylor diagrams

Taylor diagrams (Taylor, 2001) provide at-a-glance assessment of models using three different statistical metrics (standard deviation, correlation coefficient and root-mean-square difference). Figure 11 presents Taylor diagrams for select locations to compare the different methods of SSC estimation discussed: DSM2-GTM, LSTM-Standard, LSTM-Standard with precipitation, and LSTM-Standard with wind speed. These locations—Miner Slough, Jersey Point and Middle River—represent higher, intermediate, and lower performances, respectively (see Figure 10).

Important conclusions can be drawn from Figure 11. First, it is shown that including precipitation or wind speed did not drastically improve the model performance of LSTM-Standard, as indicated by the cluster of points C-E populated close to one another for all three

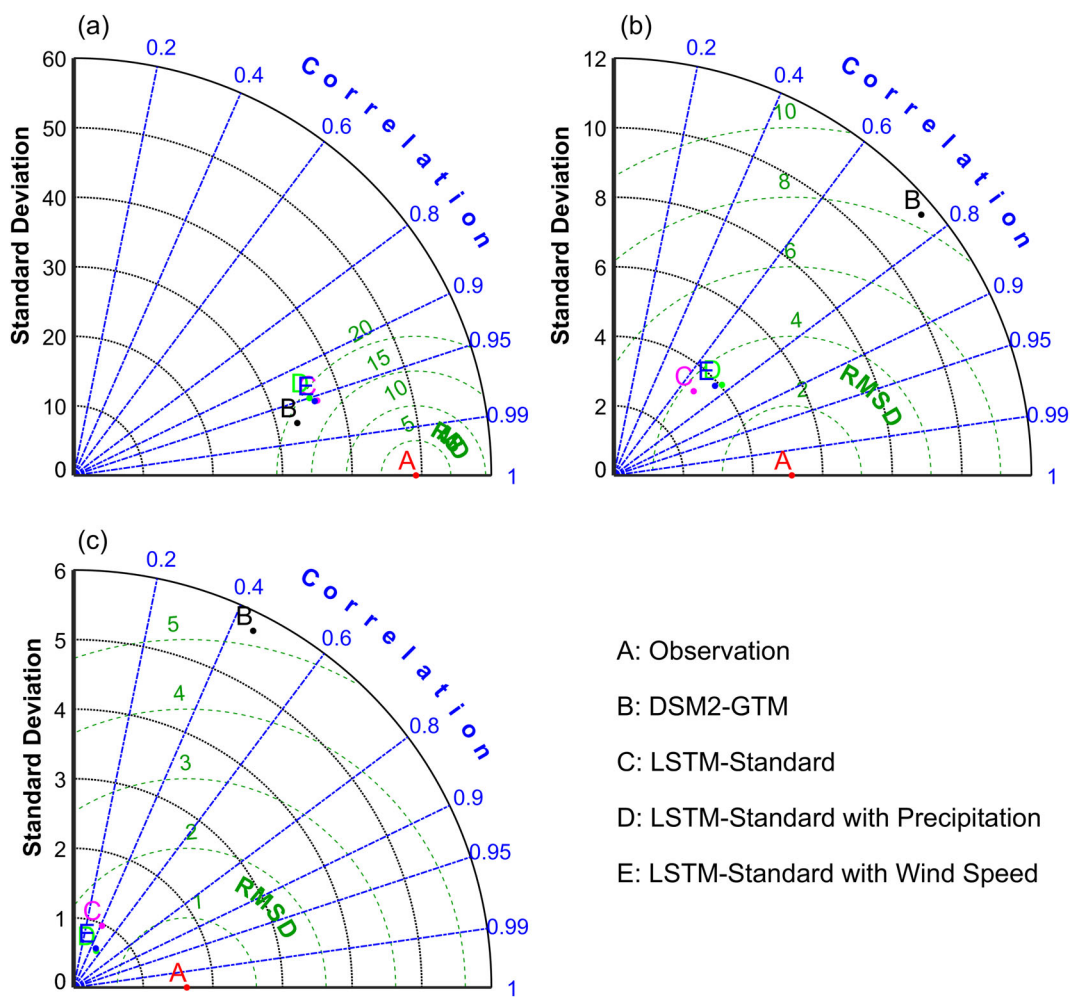


FIGURE 11 Taylor diagram comparing different suspended sediment concentration (SSC) estimation methods for (a) Miner Slough (higher performance), (b) Jersey Point (intermediate performance), and (c) Middle River (lower performance). The correlation coefficient between estimated and observed values are shown in the azimuth direction (note the change in scale at 0.90) and the standard deviation of the estimated values is indicated as the radial distance from the origin. Root-mean-square difference (RMSD) values are indicated with contours with origin corresponding to observation

locations. This is in agreement with discussions in preceding sections based on NSE values. The fact that points C-E are situated within a narrow range of standard deviation indicates that the additional inputs (precipitation and wind speed) did not significantly alter the data distribution either. Secondly, while the LSTM models and DSM2-GTM may have similar linear relationship with the observation, RMSD will help distinguish better-performing models. Case in point is shown in Figure 11c, where all methods have correlation of around 0.4. However, points C-E are associated with much lower RMSD than B, indicating the LSTM models were better than DSM2-GTM in estimating SSC. On the other hand, in Figure 11a, all points have similar RMSD, suggesting that LSTM models do not always perform better.

4.4 | Limitations

One limitation of the current study is that, like other data-driven approaches, the proposed LSTM model works as a “black box” which

is not bounded by any physical sediment transport processes. The study attempted to provide physical guidance to the LSTM model in terms of adding DSM2-GTM simulated SSC as an additional input feature to train the LSTM model (Scenarios 4 through 6). The underlying assumption was that the SSC simulations would reflect the governing sedimentation equation employed in DSM2-GTM. However, sediment transport is a complex process. Sediment supply, local storage, granulometry composition of sediments in suspension, and sediment aggradation and degradation, among other factors, all affect SSC in different ways (Hsu et al., 2019; Juez et al., 2018; Zordan et al., 2018). These factors may not be adequately represented in the governing equation of DSM2-GTM. In the future, when we collect sufficient field data that would yield a more in-depth understanding on the whole sediment transport process, we will integrate these new data to improve both DSM2-GTM and the LSTM model proposed.

In addition to incorporating simulations from process-based models as additional input features to machine learning models, recent research has embedded the governing equations of process-

based models into the loss function of machine learning models to apply physical constraints during the training process. The machine learning models developed in this way are called physics-information neural networks (PINNs) (Raissi et al., 2019). We have started developing PINNs to emulate process-based salinity models in the Delta for salinity modelling. We will extend that effort to develop PINNs for SSC modelling and report our findings in a follow-up study.

Another limitation of the study is the short amount of data available. The study aimed to emulate DSM2-GTM in SSC simulation at multiple locations in the Delta. DSM2-GTM was calibrated using three water years (2011–2013) of data and validated using another 3 years (2014–2016) of data (Hsu et al., 2019). In the spirit of emulation, we utilized the same dataset applied to calibrate and validate DSM2-GTM to train and test the LSTM models. California's hydroclimate has the largest year-to-year variability across the United States (Dettinger et al., 2011). The flow and SSC observations during 2011–2016 are most likely not representative of their counterparts in other periods. In fact, 2012–2015 was a severe drought period in California's history with record-breaking high temperature, low snowpack, and low runoff (He et al., 2017). Therefore, caution should be exercised when applying both DSM2-GTM and the LSTM models for SSC modelling during periods wetter than the period the models are calibrated or trained.

A third limitation of the study is that to fully emulate DSM2-GTM, we did not pre-process the inputs before feeding them to the LSTM models. Pre-processing inputs can improve the robustness of the machine learning model to be developed. Statistical approaches can help to identify and extract patterns in the input time series. For instance, Juez et al. (2021) utilized the wavelet transformation to capture process variability at multiple timescales for a long record of flow discharge and suspended sediment fluxes. This temporal information extracted can be used to better train the machine learning models. There have been efforts to develop hybrid wavelet and ANN models to simulate SSC (Liu et al., 2013) and other water quality variables (Alizadeh & Kavianpour, 2015). In our future work, we will explore the combination of wavelet analysis and ANNs in modelling SSC in our study area. Another pre-processing approach is to reduce the number of input variables fed into the machine-learning model and thus increase the training efficiency. Dimension reduction techniques (e.g., the Principal Component Analysis) can be employed for this purpose to identify the primary predictors for SSC. We will also explore dimension reduction methods in our future work.

4.5 | Implications

Despite those limitations, the current study has both scientific and practical implications. From a scientific standpoint, the current study is the first to explore and demonstrate the capability of deep learning networks (i.e., LSTMs) in sediment modelling in the Delta. That is, as the Delta is a very complex network of bodies of water, the successful implementation of LSTM models in this study showcased strength and efficiency of data-driven approaches. In turn, the models

developed herein would lay the foundation for other deep learning studies (e.g., for other important variables relevant to water resources management using different types of deep learning approaches) in the Delta, which is a region with tremendous economic, social, and environmental significance. While there are previous studies that involve LSTM estimation of suspended sediment transport elsewhere, they focused on localized events; Kaveh et al. (2021) used flow and sediment concentration from a single river gauge and AlDahoul et al. (2021) used two gauges along a river to obtain sediment and flow data separately. The LSTM models in this study were trained with spatially diverse measurements from 12 stations. Moreover, the effect of hydro-meteorological data (precipitation and wind speed) was also explored in the current study.

From a practical perspective, the results indicate that there is great potential for these LSTM models to supplement existing suite of process-based models for improved SSC simulation. Particularly, for locations where the performance of the process-based model is only fair (e.g., Middle River (MID) in Figure 10c), the corresponding outcome of the LSTM model can serve as a "second opinion" to inform decision-making. Additionally, running a process-based model is often time-consuming especially when the simulation period is long and when multiple scenarios need to be examined. In comparison, the trained LSTM models only take seconds to run and generate results. In this regard, the LSTM models can provide a quick peek on the big-picture information before more detailed and comprehensive estimates from the process-based model become available. Another way in which the LSTM models may be utilized is by quickly providing near-real time estimations following a disruptive event (e.g., sudden release of sediment-laden water from a reservoir). These estimations will guide decision makers with allocation of resources. In order to reach such operation-ready status, however, it is critical that the LSTM models be trained with observation records reflecting not only various hydrologic conditions but also full array of operating scenarios, taking into account gate schedules, consumptive use, and so forth, which is under development and will be reported in a follow-up study.

Lastly, the study showcased the strength and efficiency of data-driven approaches and paved the way for deep learning studies not only on sediment, but also on other important aquatic variables (e.g., flow, water temperature, dissolved oxygen, salinity, mercury, etc.) in deltaic/estuarine environments around the world. This contribution is especially timely, as sea-level rise due to climate changes places coastal communities in critical danger (Carrasco et al., 2016).

5 | CONCLUSION

The long short-term memory (LSTM) network was employed to build a data-driven tool that can estimate suspended sediment concentrations (SSC) at various locations within the Sacramento-San Joaquin Delta. The estimations are based on field observations of flow volume, stage and sediment concentrations at domain boundaries. In general, the LSTM models performed better than or as well as a process-based model in estimating SSC in terms of statistical metrics examined and

also via visual inspection of relevant simulated versus observed time series. A “hybrid” approach was also tested wherein the LSTM models were trained with local solution from the process-based model. While training with process-based model’s outputs improved LSTM model estimations in some locations, its benefits were found to be inconclusive overall, due to the small number of test scenarios. Other ways in which the LSTM models can be improved were explored by including precipitation and wind speed, which can affect sedimentation in rivers. While precipitation led to small improvement, wind speed was found to have no noticeable effects on the model performance. Nevertheless, the present study showed widened potential for machine learning techniques in hydrologic applications. Potential future research directions would include (a) the use of longer time series for training and validation, additional training datasets reflecting real-time operations, and dividing sediment into different size classes; (b) full emulation of the process-based model in terms of expanding the spatial domain (i.e., currently 12 locations) to cover the entire Delta and improving the time step (i.e., daily) to finer resolutions (e.g., 15-min); (c) development of multi-task learning networks (versus the single-task learning LSTMs developed in the current study) that can estimate suspended sediment concentrations at multiple locations simultaneously across the Delta; and (d) exploration of new machine learning architectures (including hybrid wavelet-artificial neural networks and physics-informed neural networks) and dimension reduction techniques.

ACKNOWLEDGEMENTS

The authors would like to thank Jonathan Fernandez of University of California, Davis, for his contribution to the experiment design of the study. The authors sincerely thank two anonymous reviewers for their insightful, thoughtful and constructive comments that largely helped to improve the quality of the work. The views expressed in this paper are those of the authors, and not of the State of California.

DATA AVAILABILITY STATEMENT

The data that support the findings of this study are available on request from the corresponding author.

ORCID

Han Sang Kim  <https://orcid.org/0000-0003-3983-9543>

Minxue He  <https://orcid.org/0000-0001-9229-7451>

REFERENCES

- Abadi, M., Agarwal, A., Barham, P., Brevdo, E., Chen, Z., Citro, C., Corrado, G., Davis, A., Dean, J., Devin, M., Ghemawat, S., Goodfellow, I., Harp, A., Irving, G., Isard, M., Jozefowicz, R., Jia, Y., Kaiser, L., Kudlur, M., ... Zheng, X. (2015). *TensorFlow: Large-scale machine learning on heterogeneous systems*. Software available from tensorflow.org.
- Abrishamchi, A. & Nam, K. (2019). “GTM-SED Sediment Bed Integration.” Methodology for Flow and Salinity Estimates in the Sacramento-San Joaquin Delta and Suisun Marsh. 40th Annual Progress Report from the California Department of Water Resources to the State Water Resources Control Board, Chapter 5.
- Achete, F. M., van der Wegen, M., Roelvink, D., & Jaffe, B. (2015). A 2-D process-based model for suspended sediment dynamics: a first step towards ecological modeling. *Hydrology and Earth System Sciences*, 19(6), 2837–2857. <https://doi.org/10.5194/hess-19-2837-2015>
- Afan, H. A., El-shafie, A., Mohtar, W. H., & Yaseen, Z. M. (2016). Past, present and prospect of an artificial intelligence (AI) based model for sediment transport prediction. *Journal of Hydrology*, 541, 902–913.
- AlDahoul, N., Essam, Y., Kumar, P., Ahmed, A. N., Sherif, M., Sefelnasr, A., & Elshafie, A. (2021). Suspended sediment load prediction using long short-term memory neural network. *Scientific Reports*, 11, 7826. <https://doi.org/10.1038/s41598-021-87415-4>
- Alizadeh, M. J., & Kavianpour, M. R. (2015). Development of wavelet-ANN models to predict water quality parameters in Hilo Bay. *Pacific Ocean. Marine pollution bulletin*, 98(1–2), 171–178.
- Aoula, R. E., Mhammdi, N., Dezileau, L., Mahe, G., & Kolker, A. S. (2021). Fluvial sediment transport degradation after dam construction in North Africa. *Journal of African Earth Sciences*, 182, 104255.
- Bengio, Y., Simard, P., & Frasconi, P. (1994). Learning long-term dependencies with gradient descent is difficult. *IEEE Transactions on Neural Networks and Learning Systems*, 5, 157–166.
- Bernard, P. L., Schoellhamer, D. H., Jaffe, B. E., & McKee, L. J. (2013). Sediment transport in the San Francisco Bay coastal system: An overview. *Marine Geology*, 345, 3–17.
- Bever, A. J., & MacWilliams, M. L. (2013). Simulating sediment transport processes in San Pablo Bay using coupled hydrodynamic, wave, and sediment transport models. *Marine Geology*, 345, 235–253. <https://doi.org/10.1016/j.margeo.2013.06.012>
- Brigham, O. E. (1988). *The fast Fourier transform and its applications*. Prentice Hall.
- Buchanan, P. A., & Morgan, T. L. (2014). *Summary of suspended-sediment concentration data, San Francisco Bay, California, water year 2010 Data Series 808* (p. 30). U.S. Geological Survey. <https://doi.org/10.3133/ds808>
- California Department of Water Resources (CDWR). (2016). Biological assessment for the California Water Fix. Available on: http://cms.capitoltechsolutions.com/ClientData/CaliforniaWaterFix/uploads/FIX_BA_TOC_V6.pdf
- California Water Commission (CWC). (2016). Water Storage Investment Program draft technical reference. Available on: https://cwc.ca.gov/Documents/2016/WSIP/WSIP_Draft_TechRefDoc_Compiled.pdf
- Carrasco, A. R., Ferreira, Ó., & Roelvink, D. (2016). Coastal lagoons and rising sea level: A review. *Earth-Science Reviews*, 154, 356–368.
- Choi, T.-J., Choi, J.-Y., Park, J.-Y., Um, H.-Y., & Choi, J.-H. (2018). The effects of nourishments using the grain-size trend analysis on the intertidal zone at a sandy macrotidal beach. *Journal of Coastal Research*, 85, 426–430.
- Dartnell, L. (2019). *Origins: How Earth's history shaped human history*. Basic Books.
- Davoodi, M., Sakhi, M. A., & Jafari, M. K. (2009). Comparing classical and modern signal processing techniques in evaluating modal frequencies of Masjed Soleiman embankment dam during earthquakes. *Asian Journal of Applied Sciences*, 2, 36–49.
- Dettinger, M. D., Ralph, F. M., Das, T., Neiman, P. J., & Cayan, D. R. (2011). Atmospheric Rivers, floods and the water resources of California. *Water*, 2011(3), 445–478.
- Eichmanns, C., & Schüttrumpf, H. (2020). Investigating changes in aeolian sediment transport at coastal dunes and sand trapping fences: A field study on the German coast. *Journal of Marine Science and Engineering*, 8, 1012.
- Erikson, L. H., Wright, S. A., Elias, E., Hanes, D. M., Schoellhamer, D. H., & Largier, J. (2013). The use of modeling and suspended sediment concentration measurements for quantifying net suspended sediment transport through a large tidally dominated inlet. *Marine Geology*, 345, 96–112. <https://doi.org/10.1016/j.margeo.2013.06.001>
- Fishman, M. J., & Friedman, L. C. (1989). *Methods for determination of inorganic substances in water and fluvial sediments* (p. 545). U.S. Geological

- Survey Techniques of Water-Resources Investigations, book 5, chap. A1.
- Golmohammadi, G., Prasher, S., Madani, A., & Rudra, R. (2014). Evaluating three hydrological distributed watershed models: MIKE_SHE, APEX, SWAT. *MDPI Hydrology*, 1, 20–39.
- He, M., Russo, M., & Anderson, M. (2017). (2017) Hydroclimatic characteristics of the 2012–2015 California drought from an operational perspective. *Climate*, 5, 5.
- He, M., Zhong, L., Sandhu, P., & Zhou, Y. (2020). Emulation of a process-based salinity generator for the Sacramento–San Joaquin Delta of California via deep learning. *Water*, 12(8), 2088.
- Hochreiter, S., & Schmidhuber, J. (1997). Long short-term memory. *Neural Computation*, 9, 1735–1780.
- Hsu, E., Anderson, J., Sandhu, P. (2019). “DSM2 Sediment Transport Model (GTM-SED).” Methodology for Flow and Salinity Estimates in the Sacramento-San Joaquin Delta and Suisun Marsh. 40th Annual Progress Report from the California Department of Water Resources to the State Water Resources Control Board, Chapter 4.
- Hsu, E., Ateljevich, E., Sandhu, P. (2016). “Delta Salinity Simulation with DSM2- GTM.” Methodology for Flow and Salinity Estimates in the Sacramento-San Joaquin Delta and Suisun Marsh. 35th Annual Progress Report from the California Department of Water Resources to the State Water Resources Control Board, Chapter 4.
- Hunt, B. E. (2009). *Monitoring scour critical bridges (NCHRP synthesis 396)*. Transportation Research Board.
- Jassby, A. D., Cloern, J. E., & Cole, B. E. (2002). Annual primary production: Patterns and mechanisms of change in a nutrient-rich tidal ecosystem. *Limnology and Oceanography*, 47(3), 698–712.
- Juez, C., Garijo, N., Hassan, M. A., & Nadal-Romero, E. (2021). Intraseasonal-to-interannual analysis of discharge and suspended sediment concentration time-series of the upper Changjiang (Yangtze River). *Water Resources Research*, 57, e2020WR029457. <https://doi.org/10.1029/2020WR029457>
- Juez, C., Hassan, M. A., & Franca, M. J. (2018). The origin of fine sediment determines the observations of suspended sediment fluxes under unsteady flow conditions. *Water Resources Research*, 54(8), 5654–5669.
- Kalnejais, L., Martin, W., Signell, R., & Bothner, M. (2007). The role of sediment resuspension in the remobilization of particulate-phase metals from coastal sediments. *Environmental Science and Technology*, 41, 2282–2288.
- Kaveh, K., Kaveh, H., Bui, M. D., & Rutschmann, P. (2021). Long short-term memory for predicting daily suspended sediment concentration. *Engineering with Computers*, 37, 2013–2027. <https://doi.org/10.1007/s00366-019-00921-y>
- Kim, D., Jo, J., & Choi, K. (2021). Role of rainfall-induced runoff discharge and human disturbance on the morphodynamics and sedimentation in the semienclosed macrotidal flats (Shinsi tidal flats, Korea). *Marine Geology*, 438(106522), 106522.
- Klausmeyer, K., & Fitzgerald, K. (2012). *Where does California's water come from? Land conservation and the watersheds that supply California's drinking water*. A Science for Conservation Technical Brief. An unpublished report of. The Nature Conservancy.
- Liu, Q. J., Shi, Z. H., Fang, N. F., Zhu, H. D., & Ai, L. (2013). Modeling the daily suspended sediment concentration in a hyperconcentrated river on the loess plateau, China, using the wavelet-ANN approach. *Geomorphology*, 186, 181–190.
- MacWilliams, M.L., Ateljevich, E.S., Monismith, S.G., and Enright, C. (2016). An overview of multi-dimensional models of Sacramento-san Joaquin Delta. San Francisco Estuary & Watershed Special Issue: The State of Bay-Delta Science 2016, Part 3.
- Marineau, M.D., and Wright, S.A. (2014) Effects of human alterations on the hydrodynamics and sediment transport in the Sacramento-San Joaquin Delta, California. *Proceedings of the International Association of Hydrological Sciences*, 367.
- McKee, L. J., Lewicki, M., Schoellhamer, D. H., & Ganju, N. K. (2013). Comparison of sediment supply to San Francisco bay from watersheds draining the Bay Area and the Central Valley of California. *Marine Geology*, 345, 47–62.
- Moriasi, D. N., Arnold, J. G., Van Liew, M. W., Bingner, R. L., Harmel, R. D., & Veith, T. L. (2007). Model evaluation guidelines for systematic quantification of accuracy in watershed simulations. *Transactions of the ASABE*, 50(3), 885–900. <https://doi.org/10.13031/2013.23153>
- Moriasi, D. N., Gitau, M. W., Pai, N., & Daggupati, P. (2015). Hydrologic and water quality models: Performance measures and evaluation criteria. *Transactions of the American Society of Agricultural and Biological Engineers*, 58(6), 1763–1785.
- Nienhuis, J. H., Ashton, A. D., Edmonds, D. A., Hoitink, A. J. F., Kettner, A. J., Rowland, J. C., & Törnqvist, T. E. (2020). Global-scale human impact on delta morphology has led to net land area gain. *Nature*, 577, 514–518.
- Pastor, A., Larsen, J., Mohn, C., Saurel, C., Petersen, J. K., & Maar, M. (2020). Sediment transport model quantifies plume length and light conditions from mussel dredging. *Frontiers in Marine Science*, 7, 576530.
- Prentice, J. E., Reg, I. R., Colleypriest, C., Kirby, R., Sutcliffe, P. J. C., Dobson, M. R., D'Oliver, B., Elvines, M. F., Kilenyi, T. I., Maddrell, R. J., & Phinn, T. R. (1968). Sediment transport in estuarine areas. *Nature*, 218, 1207–1210.
- Raiassi, M., Perdikaris, P., & Karniadakis, G. E. (2019). Physics-informed neural networks: A deep learning framework for solving forward and inverse problems involving nonlinear partial differential equations. *Journal of Computational Physics*, 378, 686–707.
- Rasmussen, P. P., Gray, J. R., Glysson, G. D., & Ziegler, A. C. (2009). *Guidelines and procedures for computing time-series suspended-sediment concentrations and loads from in-stream turbidity-sensor and streamflow data*. U.S. Geological Survey Techniques and Methods book 3, chap. C4, 52 p.
- Rumelhart, D. E., Hinton, G. E., & Williams, R. J. (1986). Learning representations by back-propagating errors. *Nature*, 323, 533–536.
- San Francisco Estuary Institute-Aquatic Science Center (SFEI-ASC). (2016). *A Delta renewed: A guide to science-based ecological restoration in the Sacramento-san Joaquin Delta. Prepared for the California Department of Fish and Wildlife and ecosystem restoration program. A report of SFEI-ASC's resilient landscapes program, publication no. 799*. San Francisco Estuary Institute-Aquatic Science Center.
- Schobar, P., Boer, C., & Schwarte, L. A. (2018). Correlation coefficients: Appropriate use and interpretation. *Anesthesia & Analgesia*, 126(5), 1763–1768.
- Schoellhamer, D. H., Wright, S. A., & Drexler, J. (2012). A conceptual model of sedimentation in the Sacramento-san Joaquin Delta. *San Francisco Estuary and Watershed Science*, 10(3), 1–25.
- Seymore, R. J. (1989). *Nearshore sediment transport*. Springer Science and Business Media, LLC.
- Taylor, K. E. (2001). Summarizing multiple aspects of model performance in a single diagram. *Journal of Geographical Research*, 106(D7), 7183–7192.
- Thomas, J., Joseph, S., & Thrivikramji, K. P. (2018). Estimation of soil erosion in a rain shadow river basin in the southern Western Ghats, India using RUSLE and transport limited sediment delivery function. *International Soil and Water Conservation Research*, 6, 111–122.
- Vendramini, D., de Oliveira, H., & Mortatti, J. (2018). Influence of rainfall recharge on suspended sediment yields in the Piracicaba drainage basin in southeastern Brazil. *International Journal of River Basin Management*, 16(4), 469–476.
- Wang, H., Kaisam, J. P., Liang, D., Deng, Y., & Shen, Y. (2020). Wind impacts on suspended sediment transport in the largest freshwater lake of China. *Hydrology Research*, 51, 4–832.

- World Health Organization (WHO). (2017). Water quality and health – Review of turbidity. Available on <https://apps.who.int/iris/handle/10665/254631>
- Yew, W.-T., Hashim, R., & Ng, K.-C. (2017). Experimental investigation of scour induced by twin-propeller wash. *Journal of Waterway, Port, Coastal, and Ocean Engineering*, 143(4), 1–10.
- Zordan, J., Juez, C., Schleiss, A. J., & Franca, M. J. (2018). Entrainment, transport and deposition of sediment by saline gravity currents. *Advances in Water Resources*, 115, 17–32.

How to cite this article: Kim, H. S., He, M., & Sandhu, P. (2022). Suspended sediment concentration estimation in the Sacramento-San Joaquin Delta of California using long short-term memory networks. *Hydrological Processes*, 36(10), e14694. <https://doi.org/10.1002/hyp.14694>